OPEN

Patient Specific Finite Element Modeling Outputs Outperform Clinical Metrics in Predicting Fusion Cage Subsidence

Francis H. V. Lali, MEng,[a] Kay A. Raftery, MSc,[a] Hannah Levy, MD,[b] Brett A. Freedman, MD,[b] and Nicolas Newell, PhD[a]

Study Design. Finite element (FE) analysis of retrospective clinical cohort.

Objective. To determine whether preoperative CT-derived FE model outputs can improve subsidence prediction compared with conventional clinical measurements alone in patients undergoing transforaminal lumbar interbody fusion (TLIF).

Summary of Background Data. Cage subsidence occurs in ~20% of spinal fusion patients and can lead to complications requiring reoperation. While individual risk factors are known, no validated tool integrates patient anatomy, bone quality, and implant characteristics to predict subsidence. Finite element models have been hypothesized to predict subsidence but lack clinical validation.

Materials and Methods. Patient-specific FE models were created from preoperative CT scans of 42 TLIF patients: N = 22 severe subsidence (≥4 mm); N = 20 nonsevere subsidence (< 4 mm). Vertebral geometries were segmented, and bone material properties were assigned based on Hounsfield units (HU). Cage positions from postoperative scans were registered to preoperative anatomy. Endplate and trabecular stresses and strains from FE models were compared with clinical measures using receiver operating characteristic analysis.

Results. Fifteen principal stresses and strains of the FE simulations showed significantly higher values in severely subsided patients compared with the nonsevere group. Average trabecular intermediate strain achieved the highest area under the curve score (AUC = 0.809), outperforming all clinical metrics. Peak endplate minimum principal stress (AUC = 0.775) was the second-best FE classifier. Traditional clinical measures showed lower discriminative ability: cage length (AUC = 0.797), cage width (AUC = 0.750), and cage height (AUC = 0.698).

Conclusion. Patient-specific FE model outputs significantly correlate with clinical subsidence outcomes and outperform several traditional metrics in classifying severe subsidence. Both endplate and trabecular stresses and strains are important predictors, with average values showing comparable or superior performance to peak values. Integration of FE models into the clinical workflow could provide a comprehensive preoperative subsidence prediction tool.

Key Words: finite element modelling, fusion cage, fusion cage subsidence, spine, surgery, TLIF, biomechanics, interbody fusion.

(*Spine* 2026;51:E391–E399)

Received for publication January 7, 2026; accepted March 15, 2026.
From the [a]Department of Bioengineering, Imperial College London, UK; and [b]Mayo Clinic, Rochester, NY.
The device(s)/drug(s) is/are FDA-approved or approved by the corresponding national agency for this indication.
The authors report no conflicts of interest.
Address correspondence and reprint requests to Nicolas Newell, PhD, Department of Bioengineering, Imperial College London, White City Campus, London, W12 7TA; E-mail: n.newell09@imperial.ac.uk
Supplemental Digital Content is available for this article. Direct URL citations are provided in the HTML and PDF versions of this article on the journal's website, www.spinejournal.com.

DOI: 10.1097/BRS.0000000000005698

Lower back pain affects 70% of people in their lifetime and is the leading cause of disability globally.[1,2] When conservative treatments fail, interbody fusion surgeries can restore disc height and provide spinal stability through the installation of an interbody cage.[3] While multiple fusion approaches exist, TLIF is the most common, accounting for over 50% of the US spinal fusion surgery market.[4] However, postoperative cage subsidence remains a common complication with incidence rates up to 51%.[5] This can cause nonunion, progressive spinal deformity, misalignment, and require reoperation.[6,7] As such, subsidence has been correlated with poorer patient acceptable symptom state and Oswestry Disability Index scores highlighting the clinical importance of predicting and minimizing its occurrence.[8,9]

Both patient and cage-related factors influence subsidence risk. Patient factors include body mass index (BMI), smoking, and low bone mineral density (BMD).[10–13] Meanwhile, cage-related risk factors include cage height, lordotic angle, bone-cage contact area, and cage placement.[14,15] Despite knowledge of these individual risk factors, no validated clinical tool exists to integrate patient-specific anatomy, bone quality, and implant characteristics into a single subsidence risk prediction. Some literature presents potential statistical approaches to combining risk factors to predict subsidence.[14,16,17] This study presents a mechanical approach to combining risk factors.

Finite element (FE) models offer a potential tool to predict subsidence by modeling the mechanical stresses and strains induced by cages on vertebrae. Patient-specific vertebral geometries can be segmented from CT scans, and bone material properties inferred from Hounsfield units (HU).[18,19] This enables FE simulations that simultaneously account for patient anatomy, bone quality, cage geometry, and placement factors difficult to assess jointly through clinical measurements alone.

FE models are already used in spinal instrumentation development to evaluate subsidence risk with varying factors such as lordotic angle, cage material, and different bone densities.[20–22] Such studies record outputs such as peak endplate stress, which is hypothesized to indicate subsidence risk. However, these studies have not yet been validated against clinical outcomes. Consequently, the FE outputs that best predict clinical subsidence are currently unknown.

This study aims to determine whether CT-derived FE model outputs can improve subsidence prediction compared with conventional clinical measurements alone. This will be achieved by identifying outputs of FE simulations that successfully classify postoperative subsidence and comparing their discriminative ability against traditional clinical measurements.

MATERIALS AND METHODS

Data Collection

A data set of preoperative and postoperative CT scans was collected by clinicians at the Mayo Clinic (Rochester, US) across two retrospective studies.[23,24]. All CT scans were acquired from using standardized protocols (140 kV, 280 mAs, 0.75 mm slice thickness). These were approved for research use by the Mayo Clinic institutional review board (IRB#23-003878). This data was then acquired by Imperial College London and approved for use in this study by the Science, Engineering, and Technology Research Ethics Committee (SETREC #7542982). Inclusion criteria were patients over 18 years of age undergoing lumbar TLIF surgery between 2014 and 2021 with no record of traumatic injury, malignancy, infection, prior fusions, or instrumented decompression. Patients with postoperative scans less than six months after surgery or incomplete imaging records were excluded. L5-S1 fusions were excluded because mechanical loading at this level is distinct—the sacral inclination of L5 introduces an anterior shear in addition to axial compression—thus, boundary conditions would not be standardized between patients. Patients receiving multilevel fusions or polyether ether ketone (PEEK) cages were also excluded due to radiolucency, preventing accurate segmentation. After exclusion, 42 patients remained for use in this study.

Subsidence Assessment

The full subsidence assessment method is described in Levy and colleagues. Briefly, preoperative scans were acquired as part of surgical planning at most three months before the operation date and postoperative scans were acquired six months postoperation (settings: 140 kV, 280 mAs, 0.75 mm slice thickness, 0.75×0.75×0.75 mm resolution). From the postoperative scan, subsidence at the superior and inferior endplates of each TLIF level was measured as the distance between the endplate and the maximum point of intrusion into the vertebra. This was done by two independent reviewers and averaged for the final subsidence measure. The patients were classed into two groups based on the maximally subsided endplate: severe subsidence (≥ 4 mm, $n = 22$) and nonsevere subsidence (< 4 mm, $n = 20$).

Segmentation and Meshing

Vertebral anatomies were obtained from the preoperative scans using totalsegmentator,[25] which returned binary masks of the superior and inferior vertebral bodies (without posterior elements) at the level to be fused. These masks were converted into stereolithography (stl) files in 3D-Slicer,[26] and imported into Materialize 3-matic (v18.0, Materialize, Leuven, Belgium) for alignment and meshing. Cage geometries were manually segmented from the postoperative scans in Materialize Mimics (version 26.0, Materialize, Leuven, Belgium) and similarly exported to 3-matic for meshing. A mesh of tet4 elements was created for each preoperative vertebra and segmented cage, with a target edge length of 0.75 mm. The faces of all surface elements were converted to 3D shells of 0.75 mm thickness.

Alignment

Using 3-matic, an stl-registration was performed aligning the preoperative stl with the with the postoperative (Fig. 1). This provided the spatial transformation between preoperative and postoperative positions. $[T_{\text{pre-to-post}}]^{-1}$ was then applied to the segmented cages, so they aligned with the preoperative endplates. A local coordinate system was assigned to each vertebra by computing its principal axes, with the z-axis aligned to the cranial-caudal direction, the x-axis to the anterior-posterior direction, and the y-axis to the left-right direction. To avoid initial contact, cages were then translated in the vertebral z-direction to introduce a 1 ± 0.1 mm gap with the endplates. Meshes of both vertebrae and cages were exported for FE simulation in MSC Marc (v2024.1, MSC Software, Newport Beach, CA). After alignment, the model contained the patient's bone as it was before surgery with the cage in its postoperative position.

Material Properties and Boundary Conditions

All materials were modeled as linear elastic and isotropic, consistent with other lumbar spine FE

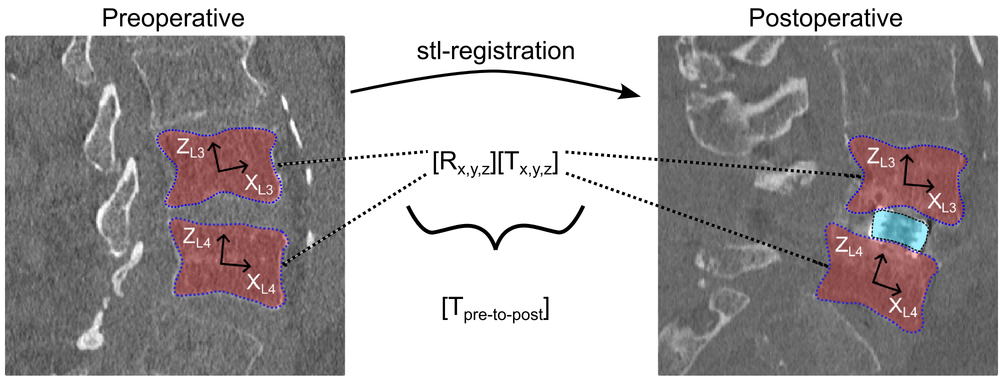

Figure 1. Illustration of preoperative and postoperative scans showing local vertebral coordinate systems and spatial transformation between them. Each vertebra was assigned an independent coordinate system. Vertebrae suprajacent and subjacent to the installed cage are highlighted red, and the cage in the postoperative CT is highlighted blue.

investigations.[27–29] The titanium cage was assigned a Young modulus 110 GPa and a Poisson ratio of 0.3.[30] To capture interpatient BMD variation, trabecular and cortical bone material properties were assigned for each patient using the mean HU of the core and peripheral bone compartments, respectively (Fig. 2). The peripheral region was defined as the volume between the original surface and a 1.5 mm inward offset, while the core region was defined as the volume within a 6 mm inward offset of the vertebra. These values were based on a preliminary sensitivity analysis showing HU converged at these values (Supplementary Figure 1, Supplemental Digital Content 1, http://links.lww.com/BRS/D47). HUs were converted to bone density and then Young modulus according to equations (1) and (2) below:[31,32]

$$\rho = 0.7 \times HU + 17.8\#(1)$$

$$E = 4730 \times \rho^{1.56}\#(2)$$

Trabecular and cortical bone were assigned Poisson ratios of 0.2 and 0.3, respectively.[30]

Cages were axially displaced through a control node (fixed in x, y, free to rotate) until the reaction force reached 50% bodyweight (Fig. 2). This simulated interpatient variability in upper bodyweight, supported by the lumbar spine.[20,33–36] Distal endplate nodes were rigidly fixed. Node-to-node touching contact with a friction

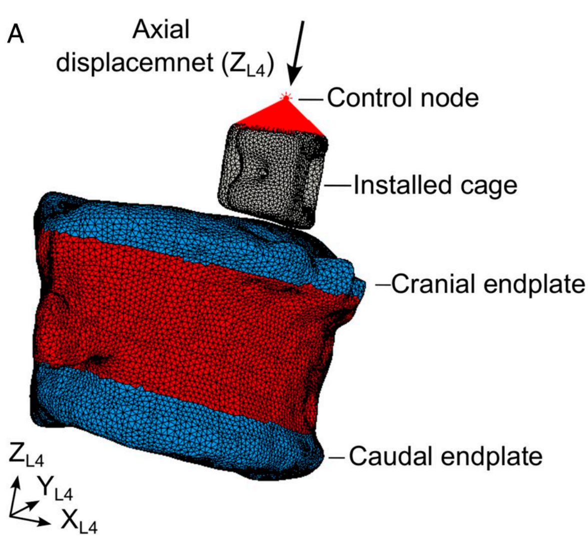

Figure 2. Finite element model setup and material property assignment. (A) Boundary conditions showing highlighted endplate regions. The inferior (caudal) endplate was rigidly constrained in all degrees of freedom. A control node coupled to the superior cage surface applied the axial compressive displacement corresponding to 50% bodyweight loading. (B) Peripheral (cortical) and core (trabecular) bone compartment segmentation. Average HU values within each compartment were used to calculate cortical and trabecular Young moduli.

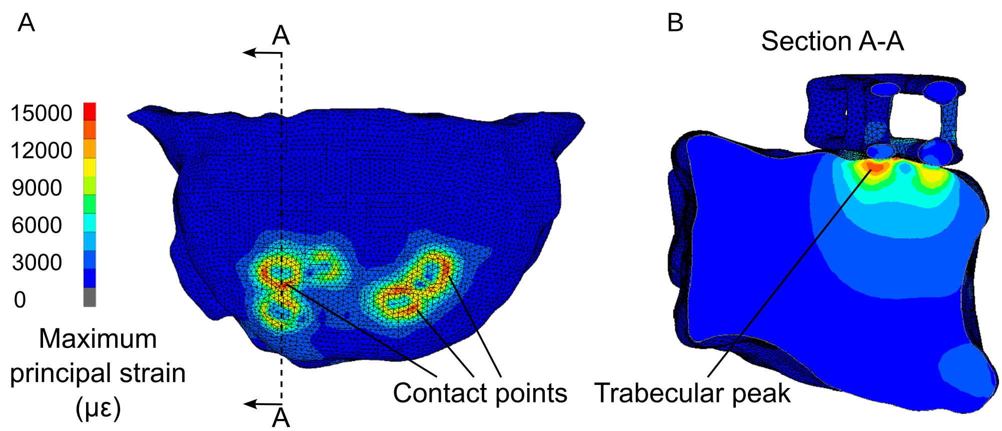

Figure 3. Finite element model setup and material property assignment. (A) Boundary conditions showing highlighted endplate regions. The inferior (caudal) endplate was rigidly constrained in all degrees of freedom. A control node coupled to the superior cage surface applied the axial compressive displacement corresponding to 50% bodyweight loading. (B) Peripheral (cortical) and core (trabecular) bone compartment segmentation. Average HU values within each compartment were used to calculate cortical and trabecular Young Moduli.

coefficient $\mu = 0.8$ was used at the nonconformal cage-endplate interface.[37,38] Cortical shells were glued to trabecular elements.

Identifying Relevant FE Outputs

One vertebral model (the maximally subsided endplate) was analysed per patient. Analyses focused on two regions of interest (ROI): (1) the endplate adjacent to the implanted cage and (2) the subcortical trabecular bone. Elements belonging to the cage and the fixed distal endplate were excluded from analysis. Six elemental scalars were considered: three principal stresses and three principal strains: σ_{max}, σ_{min}, $\sigma_{intermediate}$, ε_{max}, ε_{min}, $\varepsilon_{intermediate}$. These were selected as they represent the true maximum and minimum stress and strain states, independent of the coordinate system.

Within each ROI, both peak and average values of these scalars were assessed to determine whether local stress-strain peaks or globally distributed bone loads were better indicators of subsidence. Peak values were defined as the mean of the top 5% of element values. This avoided sensitivity to isolated element spikes that may result from mesh artefacts. Average values were defined as the median across all elements in the ROI. In total, 24 FE outputs were considered per model, six scalars, both peak and average, for two ROI's.

Comparing FE Metrics to Univariate Clinical Measures

The recorded clinical measurements were patient mass, trabecular HU, peripheral HU, cage height, cage length, cage width, cage degree of lordosis, cage type (banana or bullet), preoperative disc height, bone morphogenetic protein (BMP) use and cage height: disc height ratio. HUs were calculated from preoperative CTs by the method outlined in section 2.5. Meanwhile, cage parameters were obtained from operative notes and device implantation records. Preoperative disc height was measured from the midsagittal CT slice. The anterior, middle, and posterior heights were recorded and averaged for the final disc height.

A one-tailed independent-samples t test was performed in SPSS Statistics (Version 30.0.0.0, IBM, Armonk, NY) to identify which model outputs showed significant increases in the severe subsidence compared with the nonsevere group. To account for multiple comparisons across 24 FE outputs, a Benjamini-Hochberg false discovery rate (FDR) correction was applied to P-values with $\alpha = 0.05$. Variables that showed significant differences after correction were compared with the clinical metrics as discriminators through receiver operator characteristic (ROC) analysis. Relative values between groups were analysed rather than absolute, given that HU were uncalibrated.

ROC analysis of the significant variables and clinical measures was carried out in SPSS, providing an area under the curve (AUC) score for each variable. The AUC score indicates the variable's ability to classify severe subsidence and nonsevere subsidence groups. AUC values range from 0 to 1, where 0.5 represents random guessing and 0 or 1 represents a perfect classifier. The discrimination assessed was between severe ($n = 22$) and nonsevere ($n = 20$) subsided patients.

RESULTS

Load Distributions Resulting From Cage Compression

Figure 3 shows the maximum principal strain distribution of a typical cage-vertebra model. Due to the nonconforming shapes of concave endplates and flat cages, multiple points of contact at the cage-bone interface were frequently observed. These contact points coincided with the highest endplate stress and strain. Trabecular stress-strain peaks occurred in the subcortical region underlying these contact points.

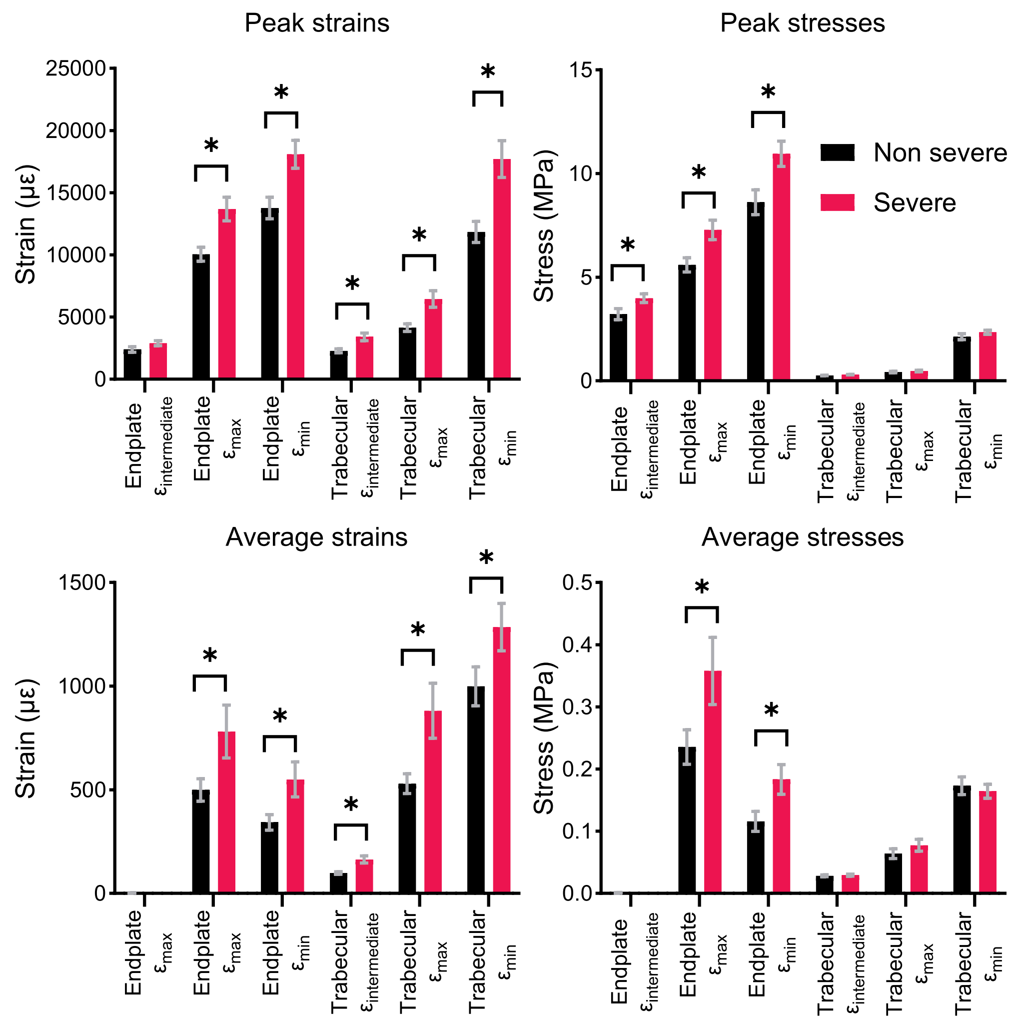

Figure 4. Mean ± SE margin of (A) peak strain means, (B) peak stress means, (C) average strain means, and (D) average stress means for each FE output. * Denotes significant difference in means after FDR correction.

Comparison of FE Outputs Between Severe and Nonsevere Groups

Figure 4 summarizes the differences between FE output means in the nonsevere subsidence and severe subsidence groups. Six trabecular and nine endplate outputs were significantly higher in the severe subsidence group.

Five of the considered stress metrics and nine of the considered strain metrics were significantly higher in the severe subsidence group as well as eight of the peak values and seven average values. Table 1 summarizes the exact values of these FE outputs by group and the multiple comparison correction used to identify significance.

Identifying Which Metrics Best Classify Severe *Versus* Nonsevere Subsidence

ROC curves of each significant FE metric are shown in Figure 5. Varying the output threshold to determine patient groups affected the sensitivity and specificity of each output differently. However, the general trend of increasing sensitivity decreasing the specificity of each output was consistent.

The AUC scores produced by each ROC curve are summarized and compared with the clinical metrics in Figure 6.

Of the clinical metrics only cage length and cage width achieved AUC scores above 0.7 which is a general threshold for an acceptable diagnostic tool.[39] $HU_{peripheral}$, cage angle, and preoperative disc height achieved the lowest AUC's ~0.5 indicating that as univariate predictors they perform similarly to a random guess.

DISCUSSION

This is the first study to compare the outputs of preoperative patient-specific FE models of fusion cages with postoperative clinical subsidence outcomes. Our results demonstrate that FE outputs previously hypothesized to be linked with subsidence are indeed correlated with patient outcomes, providing evidence that these

TABLE 1. FE Output Means ± SD for the Nonsevere and Severe Subsidence Group

	Output	Nonsevere Mean ± SD	Severe Mean ± SD	Raw P	Adjusted-α
Stresses (MPa)	Endplate σ_{min} avg	0.12 ± 0.07	0.18 ± 0.11	**0.012**	***0.021**
	Endplate σ_{max} avg	0.24 ± 0.13	0.36 ± 0.25	**0.027**	***0.029**
	Endplate σ_{max} peak	5.59 ± 1.55	7.28 ± 2.19	**0.003**	***0.015**
	Endplate σ_{min} peak	8.62 ± 2.65	11.00 ± 2.86	**0.004**	***0.017**
	Endplate $\sigma_{intermediate}$ peak	3.21 ± 1.19	3.99 ± 0.99	**0.015**	***0.023**
	Trabecular σ_{max} avg	0.06 ± 0.17	0.08 ± 0.18	0.139	0.040
	Trabecular $\sigma_{intermediate}$ peak	0.26 ± 0.07	0.30 ± 0.08	0.040	0.033
	Trabecular σ_{max} peak	0.42 ± 0.17	0.47 ± 0.18	0.182	0.046
	Trabecular σ_{min} peak	2.13 ± 0.65	2.35 ± 0.47	0.115	0.038
	Trabecular $\sigma_{intermediate}$ avg	0.03 ± 0.01	0.03 ± 0.01	0.306	0.048
	Endplate $\sigma_{intermediate}$ avg	0.00 ± 0.00	0.00 ± 0.00	0.165	0.044
	Trabecular σ_{min} avg	0.17 ± 0.06	0.16 ± 0.05	0.315	0.050
Strains (με)	Trabecular $\varepsilon_{intermediate}$ avg	88.5 ± 29.3	164 ± 79	**0.001**	***0.002**
	Trabecular ε_{max} avg	529 ± 212	881 ± 623	**0.010**	***0.019**
	Endplate ε_{min} avg	343 ± 168	550 ± 397	**0.017**	***0.025**
	Endplate ε_{max} avg	499 ± 241	781 ± 597	**0.026**	***0.027**
	Trabecular ε_{max} peak	4150 ± 1370	6450 ± 3140	**0.002**	***0.008**
	Trabecular $\varepsilon_{intermediate}$ peak	2280 ± 708	3410 ± 1470	**0.002**	***0.006**
	Trabecular ε_{min} peak	11800 ± 3810	17700 ± 6950	**0.001**	***0.004**
	Endplate ε_{max} peak	10000 ± 2500	13700 ± 4480	**0.002**	***0.010**
	Endplate ε_{min} peak	13800 ± 3890	18100 ± 5270	**0.002**	***0.013**
	Trabecular ε_{min} avg	999 ± 419	1280 ± 538	**0.031**	***0.031**
	Endplate $\varepsilon_{intermediate}$ peak	2390 ± 978	2900 ± 949	0.050	0.035
	Endplate $\varepsilon_{intermediate}$ avg	0.00 ± 6.35	0.00 ± 0.00	0.165	0.042

*Denotes adjusted-α values greater than Raw p-values. Indicated outputs are significantly different between severe and non severe subsidence group.

metrics would be useful to integrate into clinical prediction tools. Specifically, maximum, minimum, and intermediate principal stresses and strains are significantly higher in severely subsided patients (Fig. 4). These FE outputs can discriminate severely subsided patients better than some clinical measures currently available to surgeons (Fig. 6).

Previous FE investigations into cage subsidence have often used peak endplate stresses and contact pressures as indicators of subsidence risk, concluding that cage installations that induce higher stresses may increase subsidence risk.[21,40,41] This study confirms that endplate stresses are significantly higher in severely subsided patients (Fig. 4). Specifically, minimum principal stress (peak endplate σ_{min}), which was the second-best classifier of severe subsidence patients and on average 27% higher in the severe subsidence group compared with the nonsevere subsidence group. These high stress and strain regions are likely due to a nonconformal endplate-implant interface. Using this FE approach preoperatively would allow surgeons to model multiple implants and select that which has the lowest stress and strain peaks, and thus the lowest subsidence risk. Some clinical measures considered in preoperative planning were poor predictors of subsidence (preoperative disc height: 0.522, cage angle: 0.533, and peripheral bone quality: 0.543). Out of the clinical measures, cage length, width, and height were the best classifiers of severe subsidence patients with. This supports the findings of several studies that link increasing cage dimensions to subsidence.[10,42,43] Similarly, trabecular HU and patient mass had moderate discriminative power (0.661 and 0.659. respectively) which is also consistent with studies linking lower BMD and higher BMI to subsidence risk.[9,13] While this list of clinical measures is not exhaustive, and other variables may provide improved discriminative ability, this study's primary contribution is demonstrating the potential of FE modeling approaches to predict subsidence by mechanistically integrating multiple risk factors.

In addition to these findings, this data also suggests that (1) trabecular stresses and strains have similar discriminative power to endplate metrics. (2) Both peak and average stresses and strains in the endplate and trabecular region are significant indicators of subsidence. Supporting both points, the best classifier of severe subsidence patients was average trabecular $\varepsilon_{intermediate}$, which had an AUC score of 0.809 and was 66% higher in the severe subsidence group. This suggests that the average load rather than localized peaks could be better indicators of subsidence risk. Given that peaks in stress and strain are localized, heterogeneous material mapping could provide more accurate peak values and provide insight as to whether local peaks or global averages contribute more to subsidence.

The model used in this study was deliberately simplified to homogeneous linear materials, purely axial compression with no bending, and cages fixed in the x-y direction. These simplifications enabled patient specificity to be maintained and standardized across the data set, minimizing the need for manual input on model setup. However, this potentially reduces physiological accuracy, which should be the focus of future studies. Furthermore, postoperative data were used to determine cage geometry and placement; to make this completely preoperative, geometries directly from manufacturers and intended positions from surgeons could be used. This would also facilitate the inclusion of PEEK cages.

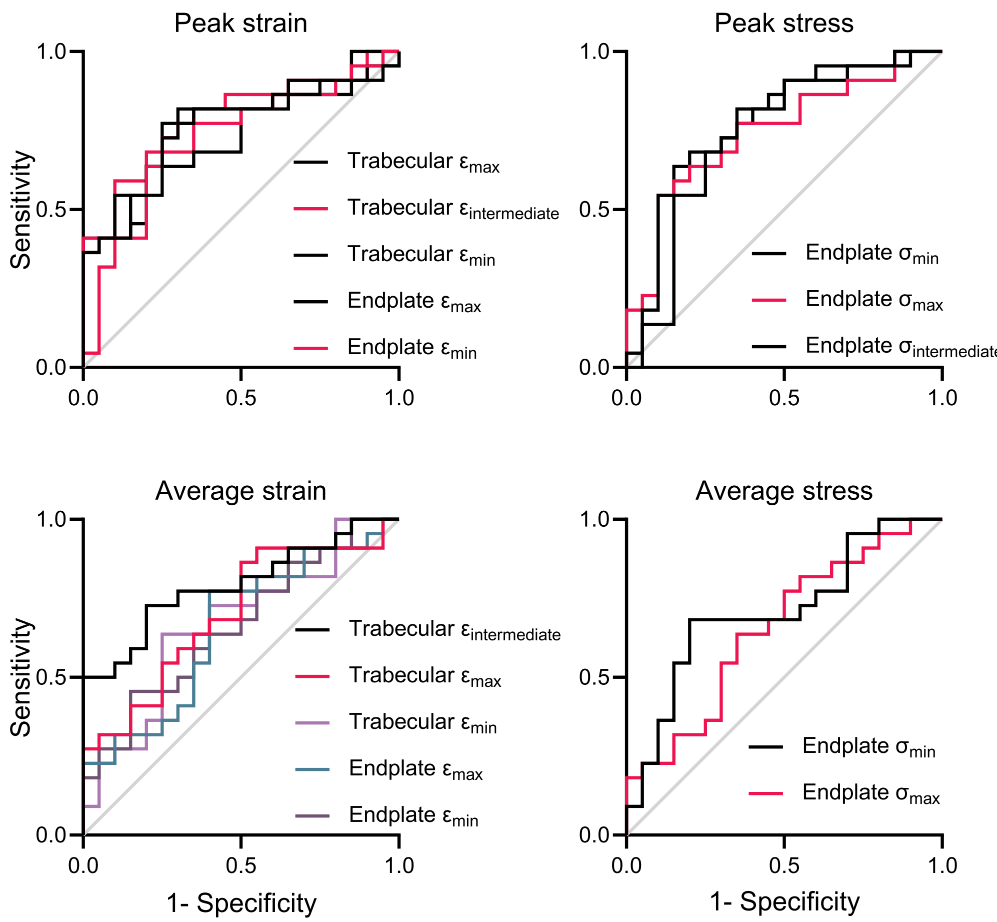

Figure 5. ROC curves for FE metrics significantly associated with severe subsidence. This includes: five of the peak principal strains; three peak principal stresses; five average principal strains; and two average principal stresses. Grey diagonal indicates equal sensitivity and specificity (random classifier performance).

Regarding loading conditions, the lumbar spine experiences complex multiaxial loading during daily activities. Stress and strain peak locations would vary under these physiological conditions, and subsidence may preferentially occur during bending, where edge loading could exceed stresses predicted by our compression-only model. To expand

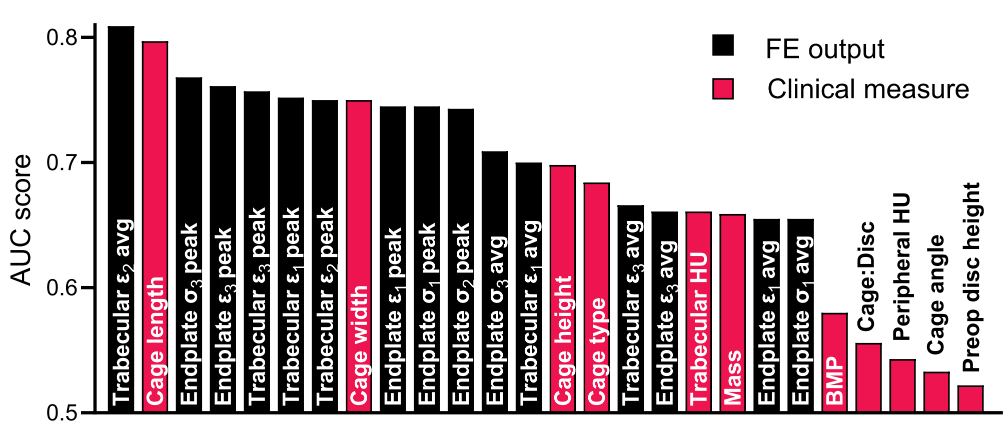

Figure 6. Area under the ROC curve for all FE parameters and clinical measures in descending order.

this modeling approach to the sacral, thoracic, and cervical spine, their respective loading conditions would need to be considered. Future models must balance increased complexity against model setup time and clinical feasibility

This study considered 42 patients, a limited sample size requiring external validation for clinical translation in larger populations with varying TLIF indications. In addition, HU values were not calibrated using standardized phantoms, limiting the comparability of absolute material property values across patients. However, our comparative analysis between subsidence groups is less affected by systematic HU offsets than the establishment of absolute clinical thresholds would be. Future clinical deployment would require calibration to ensure material property standardization. These discussed improvements would improve model accuracy and increase the sensitivity of FE outputs for predicting subsidence, providing a range of FE outputs to supplement traditional clinical metrics.

This study demonstrates that FE modeling can combine multiple patient and cage-level risk factors to provide outputs that predict subsidence better than several clinical variables. This mechanistic approach, based on physical relationships between variables, is inherently more generalizable to wider populations than statistical approaches relying on empirical correlations. Combining FE outputs with Clinical metrics should be done but with care regarding the multiple collinearities between variables. To maintain the generalisable approach offered by mechanistic model research into how to factor clinical variables as inputs to FE is necessary. This would remove some dependency on retrospective data sets; reduce risk of overfitting to small sample sizes and move toward a purely predictive tool.

This methodology could enhance preoperative planning and implant selection. Once a candidate implant is selected, an FE model could be generated and run to predict subsidence risk. Cases where risk exceeds clinically established thresholds could prompt consideration of alternative cage designs or interventions such as anabolic therapy, thereby identifying and mitigating high-risk procedures. In addition, this framework could serve as a digital twin platform to optimize cage designs and surgical technique. By running large-scale in silico trials across a range of patient anatomies, bone qualities, and implant configurations, manufacturers and researchers could systematically evaluate and refine cage designs to minimize subsidence risk before clinical deployment.

Together, these applications demonstrate a clear pathway from the validated FE outputs presented in this study to meaningful surgical decision-making.

CONCLUSION

FE modeling provides a viable platform for jointly assessing patient-level and cage-level subsidence risk factors. On the basis of the clinical validation demonstrated in this study, it is possible to develop FE-informed subsidence prediction models that could aid clinical decisions on treatment options for individual patients. These FE models—which outperformed several traditional metrics in classifying severe subsidence—should be integrated into the clinical workflow to develop a comprehensive subsidence risk prediction tool.

➢ Key Points

- ❑ Patient-specific finite element models successfully predict severe cage subsidence ($\geq$4 mm) following TLIF surgery.
- ❑ Average trabecular intermediate strain (AUC = 0.809) outperformed all clinical metrics, including cage length and width.
- ❑ Both endplate and trabecular stress/strain metrics are significant predictors, with average values performing comparably to peak values.
- ❑ FE model outputs provide a viable platform for preoperative subsidence risk assessment, integrating patient anatomy, bone quality, and implant characteristics.

References

1. Fatoye F, Gebrye T, Mbada CE, Useh U. Clinical and economic burden of low back pain in low- and middle-income countries: a systematic review. *BMJ Open*. 2023;13:e064119.
2. Andersson GB. Epidemiological features of chronic low-back pain. *The Lancet*. 1999;354:581–585.
3. Reisener M-J, Pumberger M, Shue J, Girardi FP, Hughes AP. Trends in lumbar spinal fusion—a literature review. *J Spine Surg*. 2020;6:752–761.
4. Malham GM, Wang Y-Y, Mobbs RJ. The evolving role of lateral lumbar interbody fusion in lumbar fusion: challenging the dominance of transforaminal interbody fusion. *J Spine Surg*. 2025;11:396–399.
5. Lin G-X, Kim JS, Kotheeranurak V, Chen CM, Hu BS, Rui G. Does the application of expandable cages in TLIF provide improved clinical and radiological results compared to static cages? A meta-analysis. *Front Surg*. 2022;9:949938.
6. Ko MJ, Park SW, Kim YB. Correction of spondylolisthesis by lateral lumbar interbody fusion compared with transforaminal lumbar interbody fusion at L4–5. *J Korean Neurosurg Soc*. 2019;62:422–431.
7. Rickert M, Fennema P, Wehner D, et al. Postoperative cage migration and subsidence following TLIF surgery is not associated with bony fusion. *Sci Rep*. 2023;13:12597.
8. Subramanian T, Merrill RK, Shahi P, et al. Predictors of subsidence and its clinical impact after expandable cage insertion in minimally invasive transforaminal interbody fusion. *Spine*. 2023;48:1670.
9. Yao Y-C, Chou PH, Lin HH, Wang ST, Liu CL, Chang MC. Risk factors of cage subsidence in patients received minimally invasive transforaminal lumbar interbody fusion. *Spine*. 2020;45:E1279.
10. Yao Y-C, Louie PK, McCarthy M, et al. Cage height is more important than surface area for preventing subsidence in multilevel anterior cervical discectomy and fusions. *BMC Musculoskelet Disord*. 2025;26:591.
11. Ran L, Xie T, Zhao L, Huang S, Zeng J. Low Hounsfield units on computed tomography are associated with cage subsidence following oblique lumbar interbody fusion (OLIF). *Spine J*. 2022; 22:957–964.
12. Schreiber JJ, Anderson PA, Rosas HG, Buchholz AL, Au AG. Hounsfield units for assessing bone mineral density and strength: a tool for osteoporosis management. *JBJS*. 2011;93:1057.
13. Zavras AG, Federico V, Nolte MT, et al. Risk factors for subsidence following anterior lumbar interbody fusion. *Glob Spine J*. 2024;14:257–264.

14. Xiong T, Wang B, Qin W, Yang L, Ou Y. Development and validation of a risk prediction model for cage subsidence after instrumented posterior lumbar fusion based on machine learning: a retrospective observational cohort study. *Front Med*. 2023;10:1196384.
15. Tohmeh AG, Khorsand D, Watson B, Zielinski X. Radiographical and clinical evaluation of extreme lateral interbody fusion: effects of cage size and instrumentation type with a minimum of 1-year follow-up. *Spine*. 2014;39:E1582.
16. Zhao M, Yang H, Guo S, et al. Development and validation of a predictive model and web-based calculator for cage subsidence after midline lumbar interbody fusion (midlif) surgery. *Glob Spine J*. 2025;25:21925682251383172.
17. Sun H, Tang W, Deng L, et al. Development and validation of interpretable machine learning models incorporating paraspinal muscle quality to predict cage subsidence risk following posterior lumbar interbody fusion. *Spine*. 2025;50:1375.
18. Wang H, Chen W, Jiang J, Lu F, Ma X, Xia X. Analysis of the correlative factors in the selection of interbody fusion cage height in transforaminal lumbar interbody fusion. *BMC Musculoskelet Disord*. 2016;17:9.
19. Rho JY, Hobatho MC, Ashman RB. Relations of mechanical properties to density and CT numbers in human bone. *Med Eng Phys*. 1995;17:347–355.
20. Zhang Z, Fogel GR, Liao Z, Sun Y, Liu W. Biomechanical analysis of lumbar interbody fusion cages with various lordotic angles: a finite element study. *Comput Methods Biomech Biomed Engin*. 2018; 21:247–254.
21. Chatham LS, Patel VV, Yakacki CM, Dana Carpenter R. Interbody spacer material properties and design conformity for reducing subsidence during lumbar interbody fusion. *J Biomech Eng*. 2017; 139:0510051–0510058.
22. Zou D, Yue L, Fan Z, Zhao Y, Leng H, Sun Z, et al. Biomechanical analysis of lumbar interbody fusion cages with various elastic moduli in osteoporotic and non-osteoporotic lumbar spine: a finite element analysis. *Glob Spine J*. 2024;14:2053–2061.
23. Levy HA, Pinter ZW, Reed R, et al. Transforaminal lumbar interbody fusion subsidence: computed tomography analysis of incidence, associated risk factors, and impact on outcomes. *J Neurosurg Spine*. 2024;41:463–472.
24. Levy HA, Magera CA, Messer CJ, et al. Lumbar endplate Hounsfield units enhance transforaminal lumbar interbody fusion subsidence prediction compared to trabecular Hounsfield units alone. *Glob Spine J*. 2025;16:21925682251356986.
25. Wasserthal J, Breit HC, Meyer MT, et al. Total segmentator: robust segmentation of 104 anatomic structures in CT images. *Radiol Artif Intell*. 2023;5:e230024.
26. Kikinis R, Pieper SD, Vosburgh KG. 3D slicer: a platform for subject-specific image analysis, visualization, and clinical support, . *Intraoperative Imaging and Image-Guided Therapy*In: Jolesz FA. edsNew York, NY: Springer; 2014:277–289.
27. Lee Y-H, Chung CJ, Wang CW, et al. Computational comparison of three posterior lumbar interbody fusion techniques by using porous titanium interbody cages with 50% porosity. *Comput Biol Med*. 2016;71:35–45.
28. Fang G, Lin Y, Wu J, et al. Biomechanical comparison of stand-alone and bilateral pedicle screw fixation for oblique lumbar interbody fusion surgery—a finite element analysis. *World Neurosurg*. 2020;141:e204–e212.
29. Fan W, Guo L-X, Zhao D. Stress analysis of the implants in transforaminal lumbar interbody fusion under static and vibration loadings: a comparison between pedicle screw fixation system with rigid and flexible rods. *J Mater Sci Mater Med*. 2019;30:118.
30. Wang R, Wu Z. Recent advancement in finite element analysis of spinal interbody cages: a review. *Front Bioeng Biotechnol*. 2023;11: 1041973.
31. Buenger F, Eckardt N, Sakr Y, Senft C, Schwarz F. Correlation of bone density values of quantitative computed tomography and Hounsfield units measured in native computed tomography in 902 vertebral bodies. *World Neurosurg*. 2021;151:e599–e606.
32. Morgan EF, Bayraktar HH, Keaveny TM. Trabecular bone modulus–density relationships depend on anatomic site. *J Biomech*. 2003;36:897–904.
33. Zhang Z, Li H, Fogel GR, Liao Z, Li Y, Liu W. Biomechanical analysis of porous additive manufactured cages for lateral lumbar interbody fusion: a finite element analysis. *World Neurosurg*. 2018; 111:e581–e591.
34. Erbulut DU, Zafarparandeh I, Hassan CR, Lazoglu I, Ozer AF. Determination of the biomechanical effect of an interspinous process device on implanted and adjacent lumbar spinal segments using a hybrid testing protocol: a finite-element study. *J Neurosurg Spine*. 2015;23:200–208.
35. Jiang S, Li W. Biomechanical study of proximal adjacent segment degeneration after posterior lumbar interbody fusion and fixation: a finite element analysis. *J Orthop Surg*. 2019;14:135.
36. Han K-S, Rohlmann A, Zander T, Taylor WR. Lumbar spinal loads vary with body height and weight. *Med Eng Phys*. 2013;35: 969–977.
37. Polikeit A, Ferguson SJ, Nolte LP, Orr TE. Factors influencing stresses in the lumbar spine after the insertion of intervertebral cages: finite element analysis. *Eur Spine J*. 2003;12:413–420.
38. Zhong Z-C, Wei SH, Wang JP, Feng CK, Chen CS, Yu C. Finite element analysis of the lumbar spine with a new cage using a topology optimization method. *Med Eng Phys*. 2006;28:90–98.
39. Çorbacıoğlu ŞK, Aksel G. Receiver operating characteristic curve analysis in diagnostic accuracy studies: a guide to interpreting the area under the curve value. *Turk J Emerg Med*. 2023;23:195–198.
40. Qin Y, Zhao B, Yuan J, et al. Does cage position affect the risk of cage subsidence after oblique lumbar interbody fusion in the osteoporotic lumbar spine: a finite element analysis. *World Neurosurg*. 2022;161:e220–e228.
41. Galbusera F, Schmidt H, Wilke H-J. Lumbar interbody fusion: a parametric investigation of a novel cage design with and without posterior instrumentation. *Eur Spine J*. 2012;21:455–462.
42. Igarashi H, Hoshino M, Omori K, et al. Factors influencing interbody cage subsidence following anterior cervical discectomy and fusion. *Clin Spine Surg*. 2019;32:297.
43. Kotheeranurak V, Jitpakdee K, Lin GX, et al. Subsidence of interbody cage following oblique lateral interbody fusion: an analysis and potential risk factors. *Glob Spine J*. 2023;13: 1981–1991.

